

Fatigue Behavior of ASTM A36 Steel Considering the Influence of Cutting Parameters

Rubén Becerra¹, Nelson Arzola¹ and Oscar Araque^{2,*}

¹Departamento de Ingeniería Mecánica y Mecatrónica, Universidad Nacional de Colombia, Grupo de Investigación en Diseño Óptimo Multidisciplinario, Bogotá, 111321, Colombia.

²Department of Mechanical Engineering, Universidad de Ibagué, Ibagué 730001, Colombia.

Received 22 September 2018; Accepted 11 July 2019

Abstract

The current study investigates the influence of cutting speed and feed rate of the milling process on the surface finish and the uniaxial fatigue behavior of structural ASTM A 36 steel plates. A full factorial design is proposed that considers two levels for experimental factors cutting speed and feed rate. Fatigue tests are performed with a load rate $R=0.04$ and a frequency application of 12 Hz, using a total of 32 dog bone tensile test specimens. The surface quality is characterized by measuring the mean roughness (Ra), the mean roughness depth (Rz) and the maximum roughness depth (Rmax). After several analytic methods are made, it is shown that as the cutting speed increases, surface roughness decreases. In addition, a slower cutting speed during machining increases the probability of fatigue failure survival of the material. Likewise, a greater fatigue life was found as the maximum roughness decreases (Rmax).

Keywords: surface finish, ASTM A36 steel, fatigue, feed speed, cutting speed.

1. Introduction

The incomplete understanding of the fatigue failure in structural and machine elements generated losses of at least 4% of the United States' GNP [1]. Additionally, the parameter of Surface roughness has become one of the most significant technical requirements improve the tribological properties, corrosion resistance, aesthetic appeal and fatigue strength [2].

One of the most used materials for structures is the ASTM A36 steel. Therefore, studying the ASTM A36 steel is of great importance, as it deals with the fracture to fatigue of manufactured elements with this structural steel, such as tensors hanging or suspension bridges, rods and electrical-welded mesh for reinforced concrete, folded plates for ceilings and floors, slabs, sheets and angular tubular profiles and angular, to mention some types only. Therefore, the issue in fatigue failure of components which generally ensure safety. Therefore, it is vital to analyze the fracture to fatigue so that it can be reduced, predicted, or even eliminated. Accordingly, this document develops a study of the fatigue behavior of ASTM 36- structural steel, versus four different treatments generated by the cutting parameters by milling.

Field and laboratory tests have shown that fatigue failure typically begins on areas of some type of microstructural flaw, such porosity, vacancies, inclusions, second-phase particles, plastic deformations on soft grains, residual stress incompatibility or elastic anisotropy [3]; or in regions of stress concentrations, such as changes of section, wedges, notches, wrong surface finishes, among others. The understanding of these flaws has been the subject of studies on various academic fields. There has been a general agreement that its origin in steels is due to the emergence of microcracks on

material caused by variable cyclic loads. The crack is generally split in four main stages, as represented in Figure 1. This graph describes the appearance of the fracture and a stress-life diagram (S-N).

Likewise, the effect of cutting parameters on machining has been studied throughout modern history, mainly for the milling and turning processes in steels. For instance, the research by Hayajneh et al. [5] which studies the influence of cutting parameters: rotation speed of the tool (v_n), feed speed (v_f), cutting depth (a_p) milling process on the arithmetic average roughness Ra by an analysis of variance (ANOVA), where the given model by the equation is found. (1). It can be concluded the feed speed is the most influential factor on the roughness Ra, as it turns that the lower the feed speed less, the lower value it obtained for Ra. A similar conclusion has been reached by Abdullah et al. [6]. In this latest research, their aim is to determine analytically and experimentally the effect of the machining parameters (v_f) and cutting speed (v_c) of a CNC mill machine in the Ra roughness. Finally, they determine that v_f is the most important factor on Ra, reaching the regression expression (1).

$$R_a = 1,178854 - 0,000492v_n + 0,009897v_f - 0,17625a_p - 0,000003v_nv_f + 0,000811v_na_p - 0,003012v_fa_p \quad (1)$$

On the other hand, several researches have focused to find correlations between the surface roughness and the phenomenon of fatigue. Some of them have been reported by Siebel [7] where it was found that the decrease the boundary of fatigue resistance (Se) on steels is proportional to $\log(Rt)$ when the maximum depth of the surface profile is greater than a certain critical depth of the furrow. This Rt is very close to 2 μm for tempered steels and 5 μm for annealed steels. Furthermore, it is important to mention that research in structural steels made by Koster [8] where it is concluded that,

*E-mail address: oscar.araque@unibague.edu.co

ISSN: 1791-2377 © 2019 Eastern Macedonia and Thrace Institute of Technology. All rights reserved.

doi:10.25103/jestr.123.21

in absence of residual stress influences the resistance to fatigue through the surface finish. In their presence and with a roughness within the range 2.5 – 5.0 μm, the surface finish does not significantly affect the fatigue lives. Later, Maiya & Busch [9] studied the effects of average quadratic roughness (Rq) on the fatigue of stainless steel AISI 304. The study was conducted for Low Cycle Fatigue (LCF), focusing on fatigue

life (Nf). Their results fit according to equation (2), where the fatigue life depends on the roughness Rq.

$$N(R_q) = 1,012R_q^{-0.21} \quad (2)$$

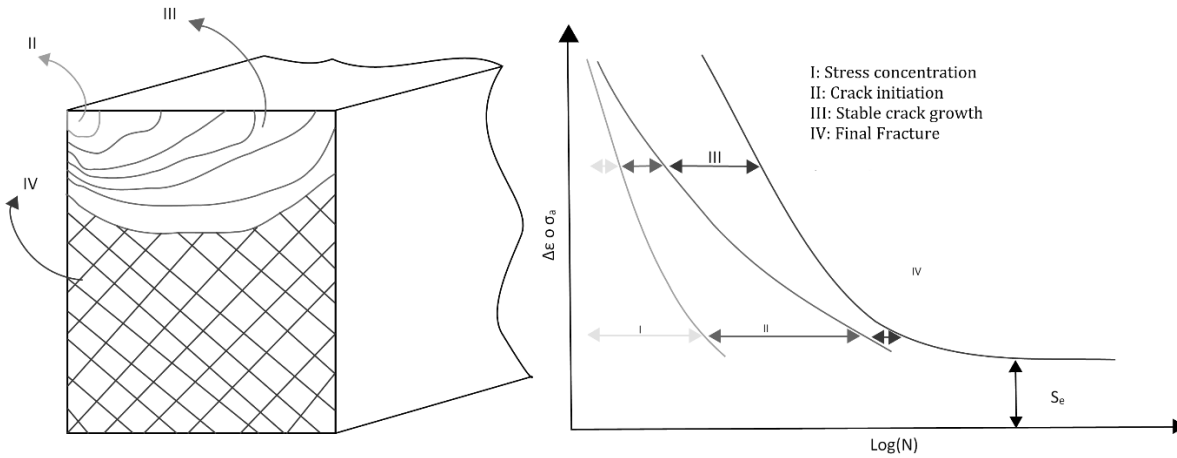


Fig. 1. Stages of fatigue failure in a common steel. Adapted from Mughrabi [4].

On the other hand, Deng et al. [10] evaluated the effect that surface roughness effect on fatigue life. To reach this, they made a three-point flexural fatigue test in notch specimen on S50C steel JIS. These were subjected to a Ra surface roughness sample and during the fatigue test, the cycle in which the crack started was found. It was done by means ohmic-sensor resistance based on coated-power cathode. Results confirm the boot cycle of crack decreases as the roughness increases. Research by Yao et al. [11] aims to optimize the milling machining of the titanium alloy Ti-10V-2Fe-3Al. It sought to reach better resistance to fatigue. To do this, they designed an three-cutting speed level experiment (vc), tooth feed speed (fz) and milling width (ac). As a response, Ra and the Rz partial roughness Rz were measured by 3D-topography with a Veeco NT1100 equipment. The dog bone-test pieces were subjected to uniaxial fatigue testing, with a load ratio equal to R=0.1 and an application frequency of cyclical load of 85-87 Hz. It can be concluded that, in terms of decreasing sensitivity: a lower fz and ac coupled with increased vc yield a better finish and a better fatigue life in a titanium alloy.

Vulliez et al. [12] correlate the roughness of the machined surface with fatigue life. To reach this, they made specimens with a ball-nose mill with angles of 45° and β = β = -3°, as for two machining paths (transverse and parallel to the load), with and without annealing. By using a confocal microscope, they took the 3D-topography from the critical area and used a recent geometrical method to measure the roughness profile based on Heron's formula with 1120 curvatures (multi-scale curvature analysis). They conclude there is a strong correlation (R² >0.96) between the obtained data by the multiple-curvature analysis and fatigue life, which translates into a new prediction method for fatigue life on machined surfaces by milling. As it relates to Huffman [13], he carried out a mathematical model by establishing a relationship between elastic energy density by external loads, energy density of dislocations and resistance to fatigue (S-N, ε - N and da/dN- and ΔK). This model becomes valid with the results of different SAE FD&E steels. The quality is worth

being highlighted, as results agree with the information organized in the diagrams S-N, ε-N and da/dN-ΔK for different values of R. It is concluded that this achieved model properly emulates the experimental data for several types of steels, aluminum, titanium, nickel alloys, copper and iron foundries. Likewise, it shows the influence of both the temperature and the hardness of the material in the fatigue life. Thus, the effects of residual stress and the machining technique become intrinsic. However, the model does not work well for low cycle fatigue.

In general, the surface roughness is not enough to estimate the fatigue life in machined metals. Even in some studies focused only on the surface roughness, as those by Moussaoui et al. [14] and Koster [8], it is shown there is not any influence over fatigue resistance and high-quality surface finishes. However, as opposed to this, Vulliez et al. [12] reach a strong model to estimate the resistance to fatigue from the surface finish generated by milling. The latter requires a censed hardware of higher quality to perform a correct statistical analysis of the superficial information that defines the finish. In addition, Zuluaga [15] shows that an inspection method through the surface finish in the CFRP composite material does not evidence a true estimate of fatigue life. It can be noted that the hardness and grain size of the material influences the fatigue life, and these vary as the manufacturing process used.

Yao et al.'s study. [16] shows that a quality-manufacturing process, such as milling, polishing, sand-blasting and re-polishing the experimental unit generates a better fatigue life, as residual compressive stresses are generated; the hardness increases, and the roughness is reduced. In addition, Novovic et al. [17] conclude that polishing after surface reciprocating grinding generates the most resistance to fatigue of their analyzed processes, including milling. Likewise, a rise on fatigue life can be observed within the samples with greater compressive residual stress, because of the machining, more than in the annealed specimen with worse surface roughness. On the other hand, Kikuchi [18] shows that using titanium can reduce the size of grain through a longer machining and to do this increases the resistance to fatigue. Parallel to a conclusion

[19] arrives Erviti, concluding that, if you give very good machining conditions followed by a correct standardization and a surface hardness enough, then Boothroyd's roughness model can be used [20]. But, as opposed to most works, this last one falls under the most influential parameter on Ra is v_c and not v_f . To conclude that, as the cutting speed increases, the exposure time to a plastic behavior gets reduced. Therefore, it has greater impact in the roughness.

The behavior of milled ATSM A36 steel to fatigue to different cutting parameters has not been studied sufficiently. Due to that fact and the importance this material poses, this work aims to study its fatigue behavior under different machining conditions, which include combinations between the parameters of feed speed (v_f) and the cutting speed (v_c). To reach this goal, a characterization about the study material through a methodology of tests based on the acquiring of composition and microstructure according to current laws. After choosing the experimental design to develop the study, the experimental ASTM A36 units are manufactured. They should have a geometry that can lead to study the phenomenon in high cycling fatigue (HCF). Finally, the characterization of the R_a , R_z and R_{max} roughness is performed on the machined sides of the specimens and the uniaxial fatigue tests are to determine uniaxial fatigue life. This procedure allowed to reach interesting conclusions about how machining parameters influence the fatigue behavior on this structural steel low-carbon content.

2. Materials and Methods

A progressive methodology was used for the ASTM A36 steel fatigue study, as shown in Figure 2. First a characterization of the base material was made. To carry it out, a metallographic and composition analysis was made to analyze the material. The mechanical properties of the material were taken from the quality certificate. Later, to study the machining process, the cutting parameters to be used for the manufacture of the specimens were defined. The cutting experimental factors were defined for two levels of study, thus a full factorial design 22 could be established. This is illustrated in Figure 3 and recorded in Table 1. However, the existence of other factors that may influence the experiments are well-known: laboratory-environment, pads and cutting tools, the cutting pattern direction, the residual stress and the initial hardness. These factors were kept constant, according to ASTM E 466. By performing this manner, a greater complexity was avoided, so it could make testing costs go higher.

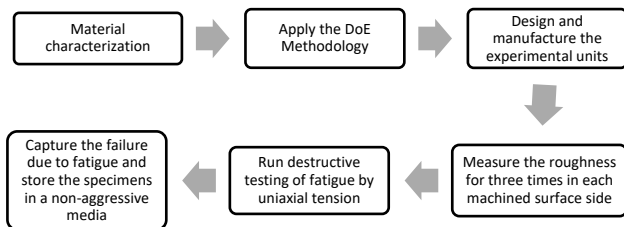


Fig. 2. Methodology used in the current study.

After, the experimental unit was designed by means of finite element analysis. A flat-geometry dog-bone specimen was selected by following the norm of ASTM E 606 model. Later, results were analytically validated along with adequate design literature and based on Marin's coefficients. By

performing this, it was guaranteed the unit had a single section of fatigue failure. Therefore, it was guaranteed a failure on the area with the surface roughness is measured. Through a finite-element analysis for the test specimens, it was validated that there is a high cycle fatigue failure (HCF) with a theoretical cycling until the failure. Such failure occurs between 10^3 and 10^5 load cycle applications. The test to fatigue in each unit ended when 10^6 cycles were exceeded, or the fatigue failure occurred.

As to estimate the number of replicas from the experimental arrangement, a variation coefficient of 5%, a difference between averages of 10% (δ); along with a statistical power of 95% and a 5% significance were considered. Bearing these considerations in mind and the use of equation (3), it was found that, at least 7 replicas for each treatment are needed. Finally, Table 1 shows the factorial experimental arrangement, where 8 selected replicas per experimental run and a total of 32 tests to be performed. The material strips to manufacture the specimens were obtained by sections. Water blats of a steel plate of 6 mm thickness by keeping their axial axis coinciding with the longitudinal direction of the plate. A random order was used for the final machining of the specimens. Likewise, roughness measurements were made and fatigue resistance tests randomly on experimental specimens.

$$r \geq 2 \left[z_{0,05} + z_{0,5} \right]^2 \left(\frac{\%CV}{\delta} \right)^2 = 2[1,96 + 1,65]^2 \left(\frac{5}{10} \right)^2 = 6.52 \tag{3}$$

Table 1. Nomenclature for the chosen experimental design.

Proof	Factor		Combination of treatment	No. replicas
	v_n [rpm]	V_f [mm/min]		
AC	1560	159	V_n low, v_f low	8
BC	1870	159	V_n high, v_f low	8
AD	1560	450	V_n low, v_f high	8
BD	1870	450	V_n high, v_f high	8

As it relates to the manufacture of each experimental unit, as dimensions are shown in Figure 3, a Leadwell CNC V-20 machining center was used to get better precision and control of the machining process. This machining center can define and monitor each of the relevant process variables related to the manufacturing. The setting up of the test specimens on the machining center can be seen in Figure 4. This illustrates a first process that reduces the size of the base material. Next, the material is machined and drilled through holes for the testing machine to be gripped. Thereunder, the machining parameters are the object of study. Therefore, they are the independent variable that will be used in the cutting tool R217.69-3240.0-18-4W ($\phi=40.0$ mm, 4 teeth and dry cutting). The rest of the cutting parameters remained fixed, i.e. a width cut a_p of 0.02 mm per pass for the final finish of the unit, an edge radius r_e of 0.8 mm and a cutting direction parallel to the load. The a_c parameter is omitted, as the pill measures 8 mm. The latter is greater than the thickness of the plate from which the specimens are obtained.

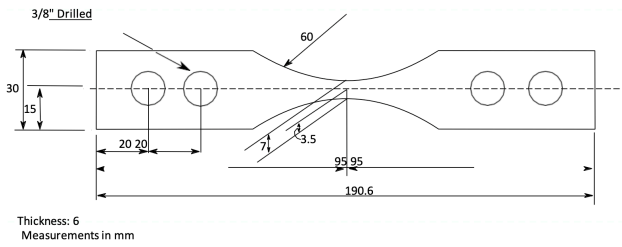


Fig 3. Dimensions of the experimental unit by taking the sample given by ASTM E 48 template

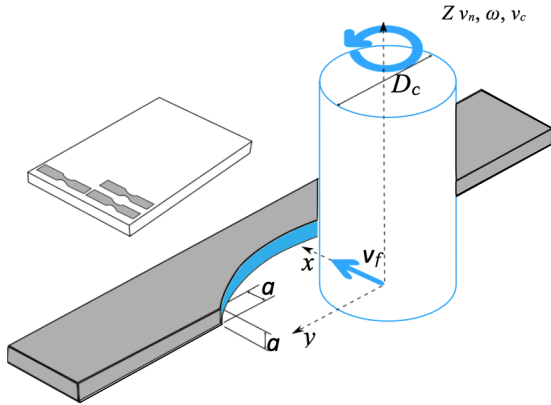


Fig. 4. Milling parameters for cutting a dog-bone flat test specimen.

After the production of the experimental units, the surface finish was measured by the Tesa Rugosurf 10G roughness meter. The latter produces the function $y(x)$ of surface roughness. As it relates to this study, special attention was paid to the arithmetic average roughness measurements (R_a), depth of the average roughness (R_z) and the maximum roughness (R_{max}). The roughness generated from the specimens were immediately recorded after being manufactured. The measurement was recorded at the center of the highest probability of failure, i.e., the neck of the experimental unit. Three measures were taken by profiled face with lengths of 5 mm, a resolution of $0.001 \mu\text{m}$ and a precision according to ISO 3274 (class 1). Yielding a total of six experimental observations per each specimens. Finally, the average of the six measures were considered. Thus, the final average values were obtained in the study for R_a , R_z and R_{max} .

As it relates to the execution of the tests, the ASTM E466 norms were followed, and a testing machine of uniaxial tension fatigue was used. The latter has an electromechanical operating principle based on a rod-crank mechanism that provides the sinusoidal loading of constant amplitude. As such, the fatigue test was defined with a maximum load of 12 kN and a minimum load of 0.48 kN, as stated in the theoretical results and computational results by FEA. Under these objectives, it was operated in HCF and with sinusoidal tension-tension stress loads, measured by a load cell type S with an application frequency of 12 Hz load cycle, within the Low Frequency Fatigue (LFF) range. The testing machine is made a continuous amplitude check of the load applied through electronic monitoring, as it must be kept within a variation of less than 2% according to ASTM E467. Likewise, the temperature around the specimen failure is monitored, as it has been verified that there is not a significant change of temperature during the experimental tests. Each test ended when a complete separation was reported or when a million load- cycles was exceeded. Likewise, the ASTM E466 requires that, in order to calculate the stress and the strength to be applied in the test, the smallest area of the test specimen must be measured with an instrument of at least 0.001 in (0.03

mm) resolution for dimensions equal to or greater than 0.200 in (5.08 mm). The latter was accomplished using a Vernier Caliper with a resolution of 0.02 mm to measure units of the neck region. As this region was found, the stress to support the neck could be projected. Therefore, the stress cycling was established with a maximum stress $\sigma_{max} = 280 \pm 2 \text{ MPa}$ and minimum stress $\sigma_{min} = 11 \pm 2 \text{ MPa}$ ($R=0.04$). After the test, the obtained data were reported according to ASTM E466 and a statistical analysis of the S-N linearization curve was made according to ASTM E739.

3. Results

Material Characterizations

Three tests were carried out by UV-VIS spark spectrometry, each in different locations of the material, thus obtaining the chemical composition of steel plate. The average results of this test are shown in Table 2. Then, a metallographic analysis is carried out, supported with an optical microscope, as shown in Figure 5. The samples were polished to get the required surface finish. Later, it was treated with Nital 3% to observe the different phases and distributions of grain in the steel. There is a 55% microstructure composed of ferrite and 45% of perlite. The latter is typical for this type of steel.

Table 2. Results of the chemical composition test.

Item	Value (%)	Item	Value (%)
Fe	98.998	Co	Less than 0.001
Si	0.2	B	0.0014
Mo	0.005	P	Less than 0.001
Al	0.053	Cr	0.03
C	0.175	Ti	0.002
Cu	0.011	Pb	Less than 0.002
W	Less than 0.005	S	0.018
Nb	Less than 0.002	V	0.001
Mn	0.484	Sn	Less than 0.001
Ni	0.018	Mg	Less than 0.000

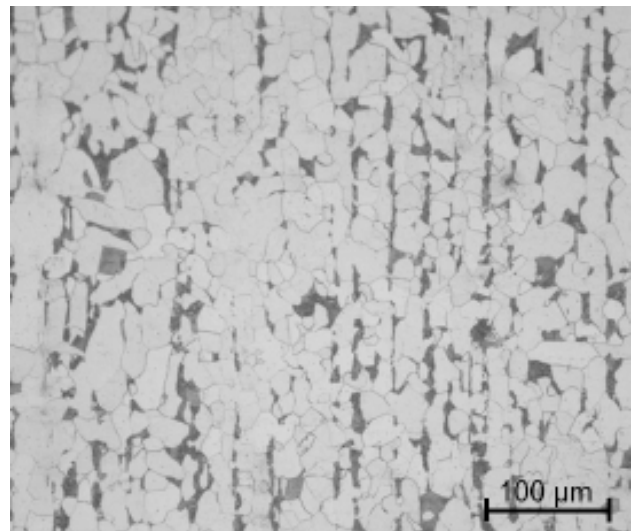


Fig. 5. Micrograph for a sample of A36 (100x) steel.

Results for the surface finish

From the results, three surfaces are obtained R^3 dependent on experimental factors in their four combinations. As to represent it, there will be a parallel cut to the plane for the cutting speed factor vs. the roughness parameter to be analyzed. This mode is carried out to observe the influence of

the cutting speed, according to the two defined levels 1560 rpm and 1870 rpm, respectively. The behavior of the arithmetic average roughness, partial z and maximum roughness with the rotation tool speed are shown in Figures 6, 7 and 8, respectively. From curves Ra, it is observed that a greater v_c and v_f it produces a lower roughness, which equates to a reduction close to $0.3 \mu\text{m}$, which is equals a percentage difference of 30%. The same trend is observed in the curve for R_{max} , where the difference between the average value of the treatment with increased surface roughness compared to one with less roughness is 20%.

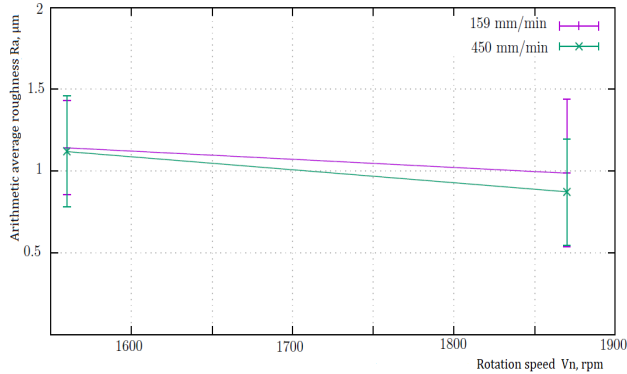


Fig. 6. Behavior of the arithmetic average roughness (R_a) with milling parameters.

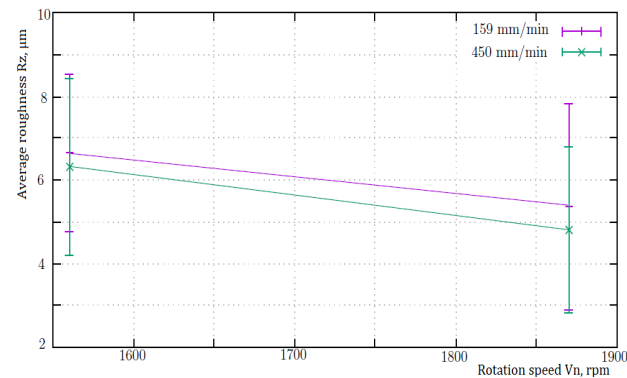


Fig. 7. Behavior of the average roughness (R_z) with milling parameters.

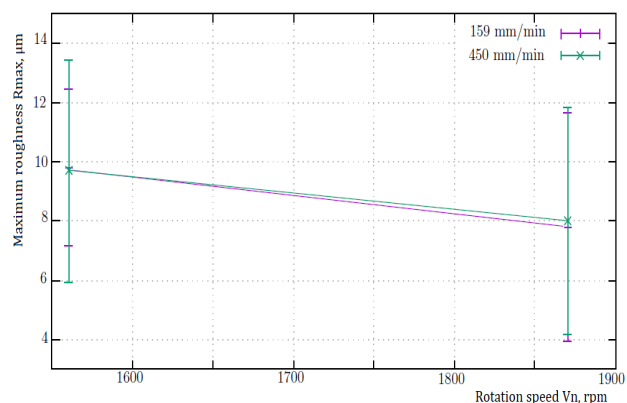


Fig. 8. Behavior of maximum roughness (R_{max}) with milling parameters.

Results for the testing of uniaxial fatigue

A compilation of the data obtained in each test to fatigue carried out to the A36 steel test specimens is presented. In Figure 9 results are shown in a S-N diagram as for the experimental results of uniaxial fatigue, along with the theoretical curve calculated with the Marin's coefficients and the confidence band considering a dispersion of $\pm 30\%$.

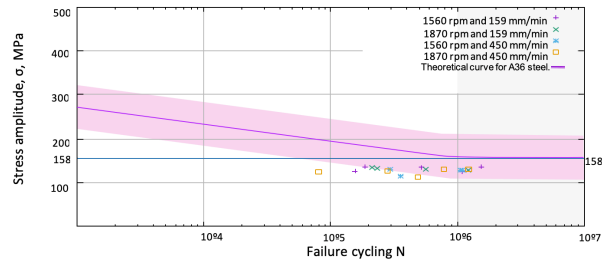


Fig. 9. Points cloud of the experimental results along with the S-N theoretical curve.

4. Discussion

Behavior of the surface finish along with the machining parameters

As with the data obtained from maximum roughness, the response surface is obtained, according to the cutting and feed speed, as the experimental arrangement was defined. It is found that the function defining the behavior of the roughness R_{max} is described, according to expression (4) with a correlation coefficient $R^2=84.6\%$. As for this behavior model of the maximum roughness, there is a contour graph shown in Figure 10. Based on this, it can be seen that the cutting speed has a greater influence than the feed speed over the maximum roughness. On the other hand, after making a visual examination of the maximum roughness dispersion, through the box-and-whisker diagram in Figure 11, it is seen their averages are not far from each other.

$$R_{\text{max}} = -5,90 + 0,074 v_f + 0,079 v_c \tag{4}$$

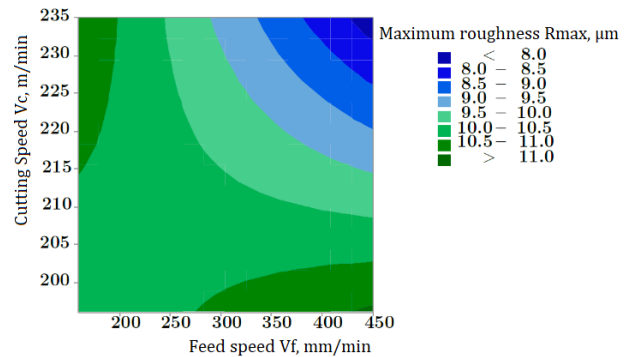


Fig. 10. Contour graph for the maximum roughness R_{max} .

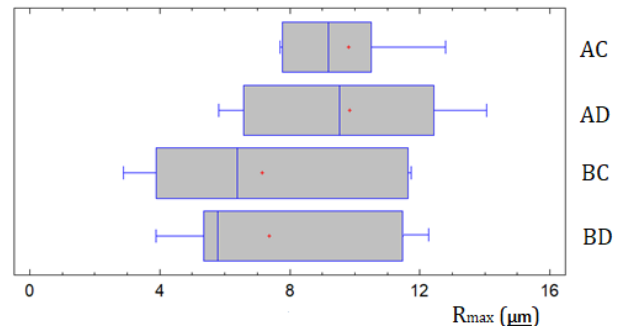


Fig. 11. Box-and-whisker diagram for the maximum roughness R_{max} for the four treatments studied.

Influence of surface finish in the fatigue life

A method used to analyze the fatigue life that do not come from a single population is recommended by Hobbacher [21]. To reach this, a load capacity is estimated (C) next to a probability of survival for all the data provided by the fatigue

tests. The load capacity is calculated according to expression (5), where m is a distribution coefficient that takes the value of 3 for steels. Later, a normal distribution of $\log C$ is generated from its average and standard deviation and is represented in a diagram of cumulative normal distribution, as shown in Figure 12. When the location on the curve of each experimental unit is observed, it is found that those with higher probability of survival were treated with a slower feed speed. Two of their two combinations and at least half of these specimens got a survival chance greater than 60%. This allows us to partially conclude that those milled specimens with a feed speed of 159 mm/min have a higher survival probability to fatigue failure. The latter is consistent with the results from other authors [22,23,13], who have found that longer machined periods generate a better machined surface integrity and a longer fatigue life.

$$\log N = \log C - m * \log \sigma_a \quad (5)$$

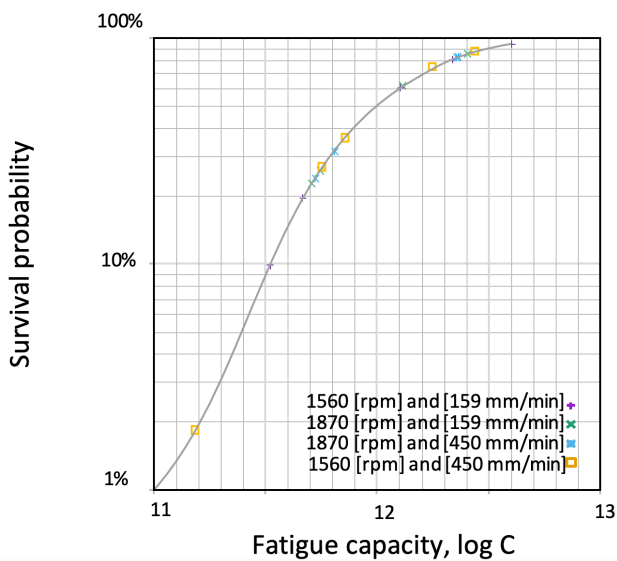


Fig. 12. Cumulative normal distribution of fatigue test results.

On the other hand, as the experimental units were taken in an arbitrary manner from those which had a greater survival probability of 23%, it can be found that treatments show a trend related to fatigue life. Figures 13, 14 and 15 illustrate that, in general, a longer fatigue life is obtained when the roughness parameters are low. In addition, there is a perceived trend of a longer fatigue life for treatments that have less feed speed ($v_f=150$ mm/min), which is consistent with the previous analysis. Likewise, there was a more consistent behavior defined by one same trend on the graphs between roughness R_{max} with fatigue life, with respect to the other measures of roughness. There was the same trend as reported by Novovic et al. [17]. This may be since R_{max} denotes the deepest discontinuity on the surface of the test specimen, which is related to the local increase of the stress and the most likely place for the emergence of a fatigue crack.

Influence of the feed speed ratio on fatigue life

The relationship between the cutting parameters is used to better identify the effect of treatment on the fatigue life. To this end, the rate between the feed speed and the rotation speed of the tool is determined, thus resulting into a feed speed rate in function of the revolutions. Figure 16 displays results, where the average value of roughness R_z for each treatment is shown.

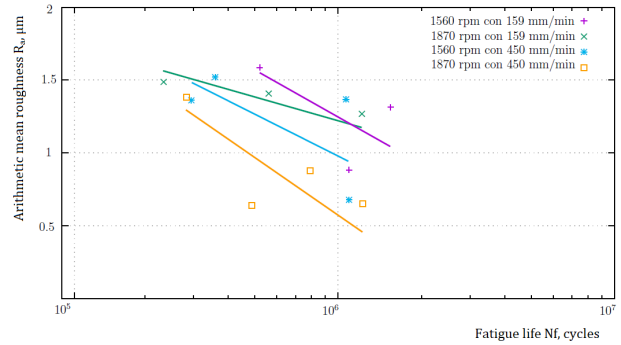


Fig. 13. Relationship between fatigue life and arithmetic mean roughness (R_a) considering milling parameters.

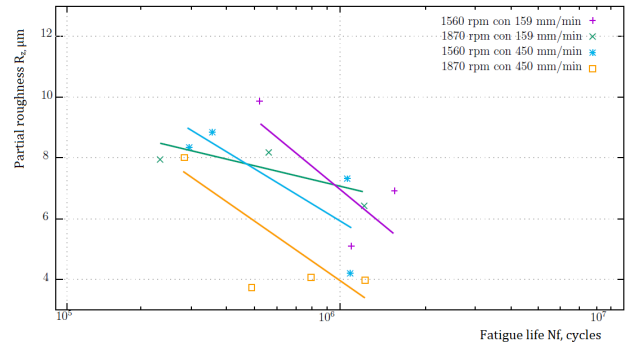


Fig. 14. Relationship between fatigue life and partial roughness (R_z) considering milling parameters.

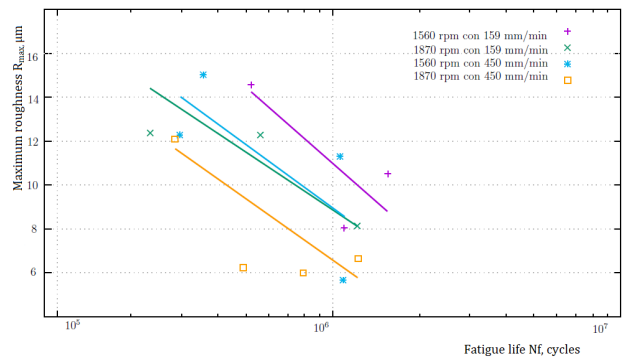


Fig. 15. Relationship between fatigue life and maximum roughness (R_{max}) considering milling parameters.

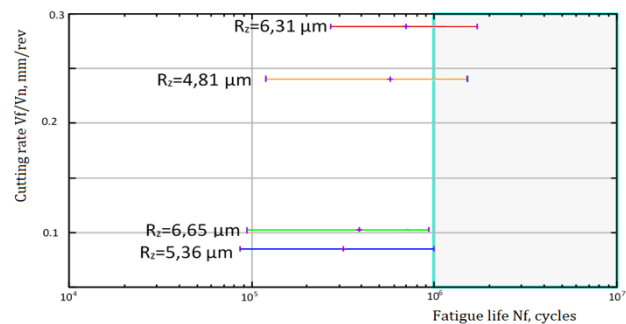


Fig. 16. Cutting rate vs. fatigue life and partial roughness.

The diagram shows that the specimens that reached a longer life to fatigue were those that experienced a higher value of the cutting rate when they were milled. The treatments which generated the greatest fatigue life in the experiment were obtained by those with a higher level of feed speed. When examining the average roughness for each treatment, it was found that those units with greater roughness got a greater fatigue life, as opposed to the common thought.

Effect of milling on the roughness measurements

For a comparative analysis has to Whitehouse [24] suggests a model of ideal roughness (R_a) around the cutting diameter of the tool and the cutting parameters v_c and v_f . After applying this information to the geometry of the cutting tool in the milling process, there is a family of curves given by equation (6). In addition, Knight & Boothroyd [25] published experimental results from the influence of the cutting speed on a turning process on a tempered steel. Thus, in Figure 17 the experimental results are represented, along with the curves defined by the latter model.

$$R_a(v_c, v_f) = \frac{0.0642}{40} \left(\frac{v_f}{v_n}\right)^2 = \frac{0.0642 \cdot 40 (v_f \pi)^2}{(4000 v_c)^2} \quad (6)$$

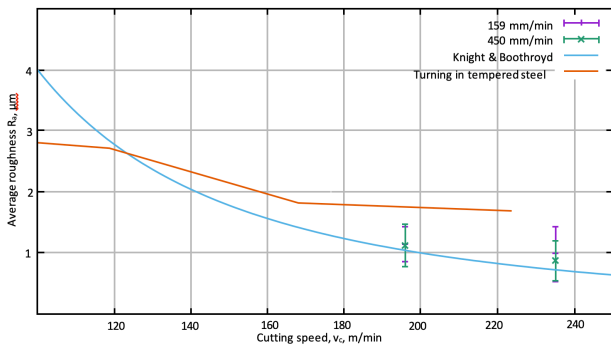


Fig. 17. Experimental results of surface roughness by turning, as stated by Knight & Boothroyd [25], along with the theoretical curve of the Whitehouse model [24] and the results of the current research.

When observing the curve for tempered steel machined by turning, it can be understood that high cutting speeds generate the roughness to remain stable. As a partial conclusion, this can be interpreted as a decrease in the natural roughness. It leaves only the ideal roughness given by the geometry of the insert, the geometry of the specimen and the machining process. In addition, it can be highlighted from the model it has a quadratic sensitivity to feed speed v_f , or, in other words, the tooth feed speed f_z . The latter is not observed graphically from the results of the experiment, but it can be noted in the family of curves from the model and the general literature. Finally, when analyzing the results obtained for the roughness, it was found that the specimens with lowest cutting speeds had a percentage difference of 7% against the ideal roughness, while the specimens with greatest cutting speeds had a percentage difference of 30% against the ideal roughness.

Effect of the roughness on the resistance to fatigue

The parameter R_t is defined as the sum of the greatest peak and the largest valley, from the roughness $y(x)$ function. However, R_z is the average of the greatest peak and valley from the division of length measurement in five stretches. So that Rodriguez [26] suggests the use approximation $R_z \approx R_t$. If this approach is adopted, it can be interpreted that the roughness generated by the experiment is close to the ideal, which would make it possible to use such an approach with a greater criterion on the results given. In such a way, by considering this approach, Siebel's results can be overlapped with [7] the experimental data that reached infinite fatigue life with its corresponding S_e , as can be seen in Figure 9. However, it should be carefully analyzed that the current research did not conduct a study on the resistance limit to fatigue of the ASTM A36 steel specimens [27].

The diagram in Figure 9 you can see that the data obtained are contained in a range of $\pm 20\%$ of the theoretical' equal to 158 MPa for the ASTM A36 steel; The latter shows a trend and allows the study to continue with historical data from Siebel. Figure 18 allows to conclude that the present study is being analyzed on the critical points of roughness, where the fatigue strength ceases to be constant and begins to be governed by the function $S_e = \log(R_t)$. Therefore, it is being studied on a range of roughness where a transition occurs in the behavior of the resistance to fatigue for steels. As a result, the behavior observed for resistance to fatigue must be analyzed by considering this transitive effect.

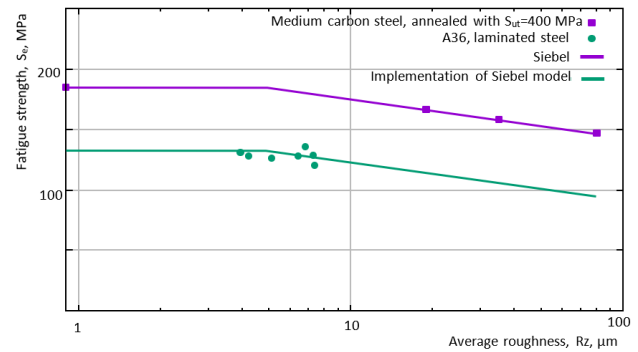


Fig. 18. Experimental results compared with the behavior reported by Siebel [7].

5. Conclusions

The executed milling process with the highest levels of cutting speed and feed speed generated a lower roughness. In terms of absolute comparison with other treatments from specimens, there is decrease in the value of roughness R_a close to $0.3 \mu m$ which is the same as the percentage difference of 30%. Likewise, between roughness R_{max} , there is a difference close to $2 \mu m$ (20%).

The cutting speed had greater influence than the feed speed on the surface roughness for the levels applied in the treatment. In addition, when comparing results with literature and historical data, it was found that the experimental conditions are in the transition region, where the roughness R_a has little variability, as an output of certain machining conditions that favor an ideal roughness. The latter is given by the geometry of the cutting tool and material properties.

The range established for the cutting parameters does not cause a large variation of the surface roughness for the material under study. After applying Siebel's model, it is concluded that the experimental results from this study are arranged near the transition glass, where fatigue strength turns from being constant to being dependent on the value for R_t .

When performing a load/fatigue capacity analysis, it can be perceived there is a trend where, as roughness R_{max} is decreased, fatigue life increases. The latter primarily occurs for the treatments with a low feed speed. However, by observing the behavior of the cutting rate (v_f/v_n), it is found that those specimens subjected to treatments with higher cutting rate showed the longest fatigue life results, even though they were not precisely the experimental units with the best surface finish.

Acknowledgment

The authors would like to thank the research office at the Universidad Nacional de Colombia and the Universidad de Ibagu e for their financial support to develop this research.

This is an Open Access article distributed under the terms of the Creative Commons Attribution License



References

- [1] N. E. Dowling, Mechanical behavior of materials: engineering methods for deformation, fracture, and fatigue, Pearson, (2012).
- [2] Kaladhar, M., Subbaiah, K. V., Rao, C., & Rao, K. N., Application of Taguchi approach and Utility Concept in solving the Multi-objective Problem when turning AISI 202 Austenitic Stainless Steel. *Journal of Engineering Science & Technology Review*, 4(1), pp. 55-61, (2011).
- [3] G. Chai, The formation of subsurface non-defect fatigue crack origins, *International Journal of fatigue*, vol. 28, No. 11, pp. 1533-1539, (2006).
- [4] H. Mughrabi, Microstructural mechanisms of cyclic deformation, fatigue crack initiation and early crack growth, *Phil. Trans. R. Soc. A*, vol. 373, No. 2038, pp. 20140132, (2015).
- [5] M. T. Hayajneh and J. Bluhm, "A study of the effects of machining parameters on the surface roughness in the end-milling process," *Jordan Journal of Mechanical and Industrial Engineering*, (2007).
- [6] A. Abdullah, L. Chia and Z. Samad, "The effect of feed rate and cutting speed to surface roughness," *Asian Journal of Scientific Research*, vol. 3, No. 4, p. 278-287, (2010).
- [7] E. Siebel, Influence of surface roughness on the fatigue strength of steels and non-ferrous alloys, *Engineers Digest*, vol. 18, pp. 109-112, (1957).
- [8] W. Koster, Effect of stress on residual fatigue of structural alloys, Residual stress Practical applications of technology, conference proceedings, Indianapolis, Indiana, pp. 1-9, (1991).
- [9] P. Maiya and D. Busch, Effect of surface roughness on low-cycle fatigue behavior of type 304 stainless steel, *Metallurgical Transactions A*, vol. 6, No. 9, pp. 1761, (1975).
- [10] G. Deng, k. Nagamoto, Y. Nakano and T. Nakanishi, Evaluation of the effect of surface roughness on crack initiation life, *Ottawa ICF12*, 2009, (2009).
- [11] C. Yao, D. Wu, Q. Jin, X. Huang, J. Ren and D. Zhang, Influence of high-speed milling parameter on 3D surface topography and fatigue behavior of TB6 titanium alloy, *Transactions of Nonferrous Metals Society of China*, vol. 23, No. 3, pp. 650-660, (2013).
- [12] M. Vulliez, M. A. Gleason, A. Souto-Lebel, Y. Quinsat, C. Lartigue, S. P. Kordell, A. C. Lemoine and C. A. Brown, Multi-scale curvature analysis and correlations with the fatigue limit on steel surfaces after milling, *Came CIRP*, vol. 13, pp. 308-313, (2014).
- [13] P. J. Huffman, A strain energy-based damage model for fatigue crack initiation and growth, *International Journal of fatigue*, vol. 88, pp. 197-204, (2016).
- [14] K. Moussaoui, M. Mousseigne, J. Senatore and R. Chieragatti, The effect of roughness and stresses on residual fatigue life time of an alloy of titanium, *The International Journal of Advanced Manufacturing Technology*, vol. 78, No. 1-4, pp. 557-563, (2015).
- [15] P. Zuluaga-Ramírez, M. R. R. Frövel, R. Trallero, R. Atienza, J. M. Painted and F. Salazar, Consumed fatigue life assessment of composite material structures by optical surface roughness inspection, *Key Engineering Materials*, vol. 559, pp. 88-95, (2013).
- [16] C. Yao, L. Wu, Z. Tan and J. Zhang, Surface integrity evolution and fatigue evaluation after milling mode, shot-peening and polishing mode for TB6 titanium alloy, *Applied Surface Science*, vol. 387, pp. 1257-1264, (2016).
- [17] D. Novovic, R. Dewes, D. Aspinwall, W. Voice and P. Bowen, The effect of machined topography and integrity on fatigue life, *International Journal of Machine Tools and Manufacture*, vol. 44, No. 3, pp. 125-134, (2004).
- [18] S. Kikuchi, H. Imai, Y. Nakai, M. Ota and A. Ueno, Effect of harmonic structure design with bimodal grain size distribution on near-threshold fatigue crack propagation in Ti-6Al-4V alloy, *International Journal of fatigue*, vol. 92, p. 616-622, (2016).
- [19] A. G. Erviti Lara, Influence of cutting parameters in the Surface Roughness in the processes of milling, Thesis Universidad de Sevilla, (2015).
- [20] G. Boothroyd, *Fundamentals of metal machining and machine tools*, vol. 28, CRC Press, (1988).
- [21] A. Hobbacher and others, *Recommendations for fatigue design of welded joints and components*, Springer, (2009).
- [22] Y. Murakami and M. Endo, Effects of defects, inclusions and inhomogeneities on fatigue strength, *International Journal of fatigue*, vol. 16, No. 3, pp. 163-182, (1994).
- [23] A. Gómez Parra, A. Sanz Lobera and M. Marcos Bárcena, Preliminary analysis of the influence of the process of turning in the life to fatigue of the Aluminum Alloy UNS TO92024-T351, *Aeronautical*, (2009).
- [24] D. J. Whitehouse, *Handbook of Surface Metrology*, CRC Press, (1994).
- [25] W. A. Knight and G. Boothroyd, *Fundamentals of Metal Machining and Machine Tools*, Third Edition, (2005).
- [26] J. Rodríguez, Chapter 3: Fatigue failure, [online]. Available: <https://123idm123.files.wordpress.com/2016/09/cap-3-fallas-por-fatiga.pdf>. [Last access: 2452018].
- [27] O. Araque, N. Arzola, & O. Varón, Computational modeling of fatigue crack propagation in butt welded joints subjected to axial load, *PloS one*, 14(6), pp. 1-17, (2019).

List of symbols

Symbol	Term	Unit
a_c	Milling width	Mm
a_p	Milling depth	mm
δ	Mean difference	%
CV	Coefficient of variation	%
D_c	Cutting tool diameter	mm
F_z	Cutting speed per tooth	Mm/min
N	Fracture cycle	1
R	Load rate	1
R_a	Arithmetic mean roughness	μm
R_{max}	Maximum roughness	μm
R_q	Average quadratic roughness	μm
R_t	Total roughness	μm
r_e	Edge radius of the insert	mm
R_z	Partial roughness	μm
S_e	Resistance to fatigue	MPa
Nf	Fatigue life	Cycles
v_c	Cutting speed	m/min
V_f	Feed speed	mm/min
v_n	Rotation speed	rpm
σ_{To}	Amplitude stress	MPa
σ_{Max}	Maximum stress	MPa